

# Identification of Ru/Ceria among single atom ceria catalysts as a stable and superior material for abatement of diesel and gasoline engine pollutants

Konstantin Khivantsev,<sup>a\*</sup> Nicholas R. Jaegers,<sup>a</sup> Libor Kovarik,<sup>a</sup> Jinshu Tian<sup>a</sup>, Xavier Isidro Pereira Hernandez,<sup>a</sup> Yong Wang<sup>a,b\*</sup> and János Szanyi<sup>a\*</sup>

[a] Dr. Konstantin Khivantsev, Dr. Libor Kovarik, Dr. Nicholas R. Jaegers, Dr. Jinshu Tian, Dr. Xavier I. Pereira Hernandez, Dr. Yong Wang, Dr. Janos Szanyi, Institute for Integrated Catalysis  
Pacific Northwest National Laboratory  
Richland, WA 99352 USA  
Emails (correspondence to): Konstantin.Khivantsev@pnnl.gov, Yong.Wang@pnnl.gov, Janos.Szanyi@pnnl.gov,

[c] Dr. Yong Wang, Voiland School of Chemical Engineering and Bioengineering  
Washington State University  
Pullman, WA 99164 USA

Supporting information for this article is given via a link at the end of the document

**Abstract:** Atomically dispersed transition metals (Ru, Pd and Pt) have been prepared on CeO<sub>2</sub> and evaluated for NO<sub>x</sub>/CO abatement applications for diesel and gasoline engines, such as low temperature passive NO<sub>x</sub> adsorption (PNA), NO and CO oxidation, and three-way-catalysis (TWC). 0.5 wt% Ru/CeO<sub>2</sub> catalyst (Ru is ~27 and ~7 times cheaper than Rh and Pd) shows remarkable PNA performance, better than 1 wt% Pd/Zeolite: it achieves 100% removal of NO<sub>x</sub> during vehicle cold start. FTIR measurements reveal the formation of stable Ru(NO) complexes as well spill-over of NO to CeO<sub>2</sub> surface via the Ru-O-Ce shuttle, explaining high NO storage. Notably, Ru/ceria survives hydrothermal aging at 750 °C without loss of PNA capacity. It is also a robust NO oxidation catalyst, considerably more active than Pt or Pd/CeO<sub>2</sub>. Expanding the repertoire of Ru/CeO<sub>2</sub> catalytic applications, we further find 0.1 and 0.5 wt% Ru/CeO<sub>2</sub> to be excellent TWC catalysts, rivaling best single-atom Rh supported materials. Our study pushes the frontier of precious metal atom economy for environmental catalysis from uber expensive Rh/Pd/Pt to more sustainable cheaper Ru and highlights the utility of single-atom catalysts for industrially relevant applications.

Air pollution is one of the main issues to tackle in environmental science and catalysis [1-3]. Deteriorating air quality is directly related to toxic NO<sub>x</sub> emissions, the majority of which are produced by vehicles exhaust. Clearly, there is a continuing need to decrease emissions from diesel and gasoline engines. Within the last decade, the ammonia selective catalytic reduction (SCR) technology was implemented on the large scale by BASF on the basis of Cu/SSZ-13 materials [4,5]. The ability of Cu/zeolites to scrub NO<sub>x</sub> in the presence of sacrificial ammonia was first discovered in Japan in the 1970s [6] for Cu/FAU zeolite. However, FAU framework is hydrothermally unstable and cannot be used in emissions control applications because the steam the sample is exposed to reaches up to 700 °C during periodic diesel particulate filter (DPF) regeneration. Invention of SSZ-13 that can survive hydrothermal aging up to 750 °C and supporting isolated copper ions in the micropores of SSZ-13 were a remarkable advance that allowed to solve most emissions problems at temperature >180 °C. At this temperature sacrificial ammonia can be successfully dosed and the best SCR catalysts perform satisfactorily at this

temperature. However, during vehicle cold-start and idle operation the temperatures of exhaust are lower (~100-120 °C) and no known catalyst can catalyze NO<sub>x</sub> removal at this temperature. In order to circumvent this important issue and trap significant NO<sub>x</sub> emissions during cold start, low-temperature passive NO<sub>x</sub> adsorber (PNA) formulations have been disclosed in the last few years [7-26]. These formulations can store NO<sub>x</sub> at low temperatures (~100 °C) and release them continuously at higher temperatures > 180 °C when Cu/zeolite SCR catalysts become active. Among the first formulations platinum dispersed on gamma-aluminas, Pd and Pt oxide nanoparticles on ceria-containing materials [17,18] were evaluated. Unfortunately, those materials store only relatively low amounts of NO<sub>x</sub> and not always hydrothermally stable. The Jonson-Matthey team, first, and then others reported Pd/zeolite formulations [7-26] on SSZ-13, BEA and ZSM-5 zeolites, with considerable NO<sub>x</sub> storage at 100 °C and release above 200 °C. We recently optimized those formulations and produced high loadings of atomically dispersed Pd(II) species in zeolites SSZ-13, SSZ-39 BEA and FER which as we showed turned out to be the truly active NO<sub>x</sub> storage sites [8-11, 13, 15, 19]. We revealed that the low-temperature PNA performance of the best Pd/SSZ-13 and Pd/BEA materials is largely due to formation of a stable mixed carbonyl/nitrosyl palladium complex, Pd(II)(NO)(CO) both on Pd/SSZ-13 and Pd/BEA [8-11]. The zeolites used have to be, however, hydrophilic enough (i.e. contain enough Al) to allow all the Pd to go in the micropore and the best formulations contained high densities of super-electrophilic Pd(II)/2Al sites [8-11] where Pd is held by proximal Al pairs. Pd(II)-OH sites themselves, however, were found to also be effective for storage of NO. The common features of these materials were the presence of atomically dispersed Pd and hydrothermally stable zeolite frameworks with enough framework Al atoms to stabilize atomically dispersed Pd.

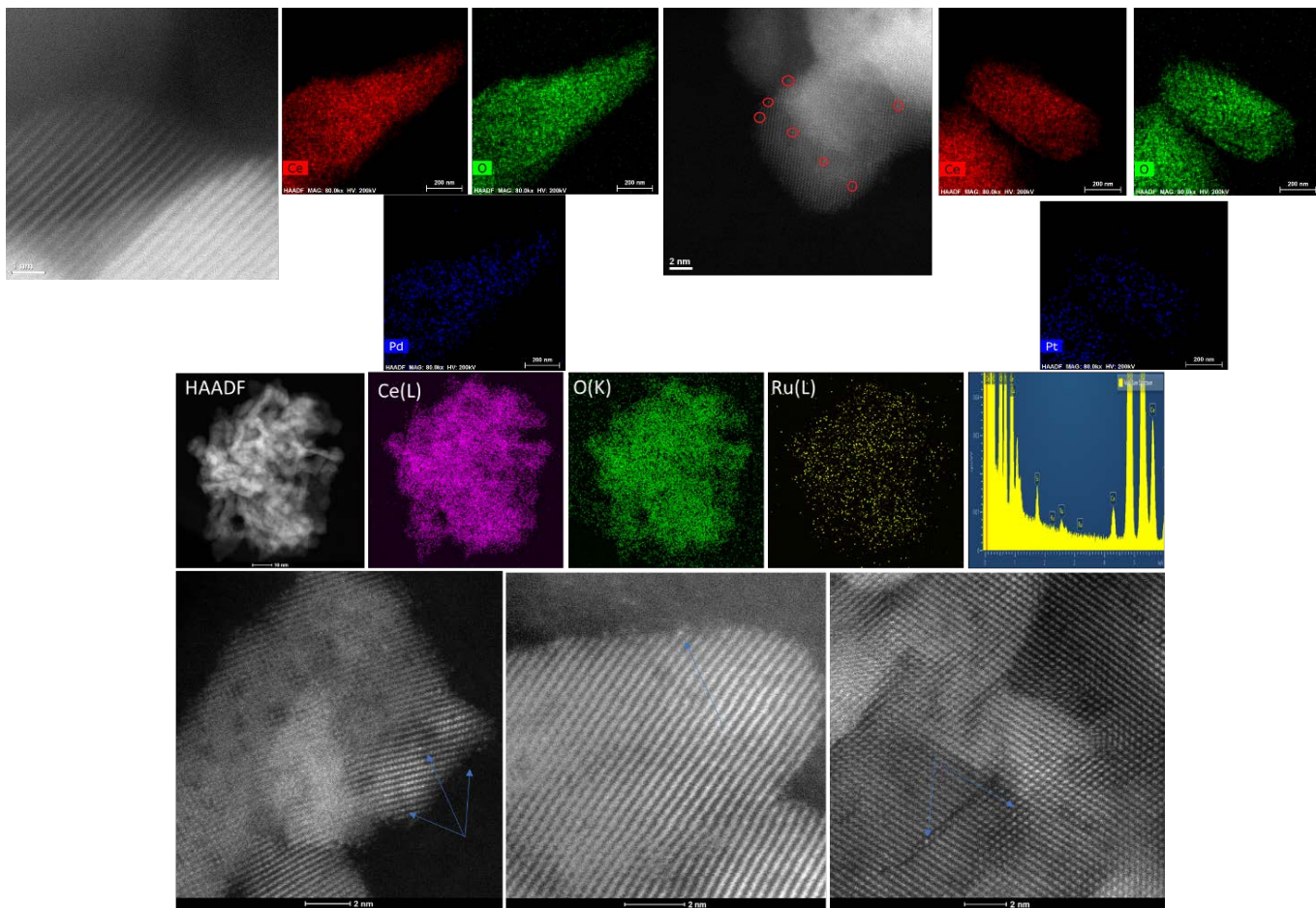


Figure 1. HAADF-STEM images and corresponding EDS maps of 0.5 wt% Pd/CeO<sub>2</sub>, 1wt% Pt/CeO<sub>2</sub> and 0.5 wt% Ru/CeO<sub>2</sub>. Single Pt and Ru atoms are highlighted with red circles and blue arrows, correspondingly.

Our early formulations of Pd/SSZ-13 could survive hydrothermal aging at 750 °C without significant loss of NO<sub>x</sub> capacity [13]. We also optimized BEA zeolite crystals to be hydrothermally stable after 750 °C aging and produced Pd/BEA materials that survived hydrothermal aging at 750 °C with no loss of NO<sub>x</sub> storage [9]. Recently, we revealed the most hydrothermally stable known Pd/SSZ-39 and Pd/FER PNAs that can survive hydrothermal aging at 800 °C in 10% H<sub>2</sub>O/air mix with basically no loss of storage capacity [15,27]. These notable findings put Pd/zeolite materials at the frontier of environmental NO<sub>x</sub> abatement field.

They show excellent NO<sub>x</sub> adsorption behavior during continuous cycle, are regenerable and remarkably survive HTA at 750-800 °C.

However, there is one main issue with wide-spread use of these materials: their price! Making zeolites is expensive because of expensive and custom-made structure-directing agents utilized for their synthesis. Moreover, the demand for Pd increased its prices significantly: currently, 1 ounce of Pd costs ~2,037 USD. On the other hand, there have been recent advances in the synthesis of thermally stable atomically dispersed Pt materials on

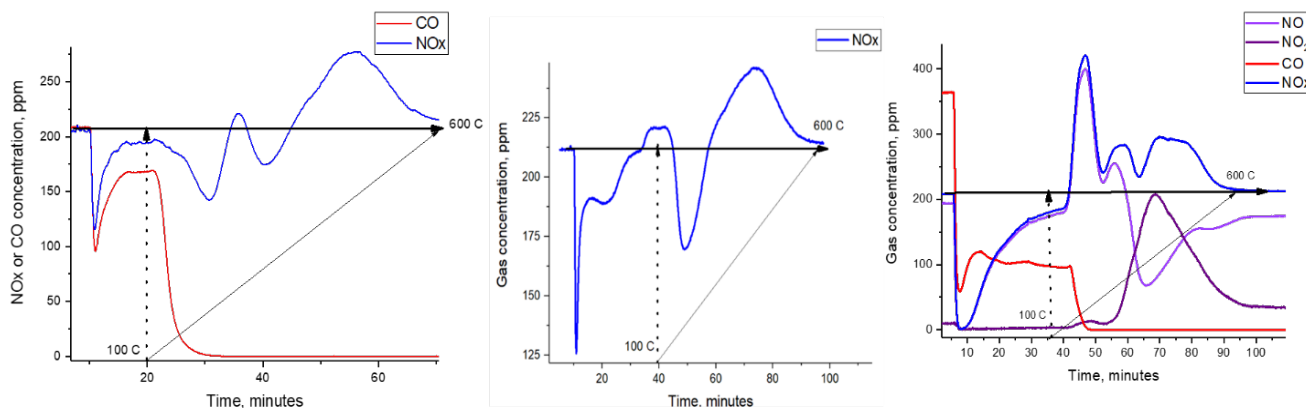


Figure 2. PNA Performance of A. 0.5 wt% Pd/CeO<sub>2</sub> B. 1 wt% Pt/CeO<sub>2</sub> C. 0.5 wt% Ru/CeO<sub>2</sub>. Catalyst mass 120 mg. Total flow rate 300 sscm/min. ~200 ppm NO<sub>x</sub>, 13% O<sub>2</sub>, 3% H<sub>2</sub>O, ~200 (or 360 ppm CO) balanced in N<sub>2</sub>. Adsorption experiments were performed at 100 °C. Vertical dashed line indicates when the ramp (10 K/min) was started.

ceria. Such materials have been prepared via novel atom trapping approach at 800 °C and were revealed to have interesting stability and catalytic properties in CO oxidation [28-31]. We note that Pt, for example, costs ~850 USD per ounce, making it cheaper on the molar basis than Pd. We also turned our attention to another transition metal Ruthenium whose price is only ~280 USD per ounce and whose molecular weight is similar to that of Pd and Rh (Rh, on the other hand, costs ~7,500 USD per ounce, almost ~27 times more on the molar basis than Ru). Taking advantage of the atom trapping approach, we prepared isolated Pd, Pt and Ru atoms on ceria in approximately equivalent molar amounts (atom loading per surface area of ceria) with 1 wt% Pt and 0.5 wt% Ru and 0.5 wt% Pd on ceria. We note that ceria material with isolated Ru atoms have not been prepared or characterized before via the described method.

We observed pronounced stabilization of ceria surface area after heating at 800 °C and producing atomically dispersed M/Ceria materials as opposed to undoped ceria (Tab. S1). This means that ceria doping with these metals produces stable materials that can survive heating in air at 800 °C. HAADF-STEM imaging of Pd, Pt and Ru supported ceria materials (Fig. 1A-C) shows crystalline ceria nanoparticles with the absence of Pt, Pd and Ru containing nanoparticles. In the case of Pt on ceria we can identify single Pt atoms located on the surface of ceria (Fig. 1B) due to higher Rutherford scattering (intensity  $\sim Z^{1.7}$ ) of Pt compared to ceria. However, in the case of Pd and Ru the contrast is poor, and we cannot clearly observe single Pd atoms (atomic numbers of Ru, Pd, Ce and Pt are 44, 46, 58 and 78 respectively). In the case of ruthenium/ceria, on sufficiently thin parts of ceria nanoparticles, we could in fact identify single Ru atoms (pointed by arrows on the surface of different ceria crystallites in Fig. 1C). However, in all 3 cases, EDS maps clearly reveal presence of Pd, Pt and Ru well-dispersed throughout the sample, further confirming our suggestion of the atomic dispersion of the said metals on ceria. Because we recently showed that Pd single atoms in zeolites are excellent low-temperature PNA adsorbers, we tested the PNA performance of Pd/Ceria for PNA first (Fig. 2A). Although it can store some amount of NO<sub>x</sub> (relatively small, ~ 20 micromoles/gram), its NO<sub>x</sub> release profile is rather convoluted and precludes its use as a passive NO<sub>x</sub> adsorber (Fig. 2A). We then tested Pt on ceria and observed similarly relatively poor performance (Fig. 2B). To our surprise, when we tested the most inexpensive 0.5 wt% Ru/ceria sample, we observed excellent PNA performance under industrially relevant testing conditions in

the presence of carbon monoxide, oxygen and water steam (Fig. 2C). During simulated cold start, the sample showed facile and complete abatement of NO<sub>x</sub> to essentially zero for ~180 seconds (which is ~ 1.8-2 times the cold start duration) (Fig. 2C). Simultaneously, the CO level (Figs. 2C) dropped from 360 to 50 ppm during adsorption and was oxidized to CO<sub>2</sub> in the presence of water with CO level ~100 ppm at 100 °C (~70% conversion). Moreover, the Ru/ceria sample showed 90% conversion of CO in the presence of NO<sub>x</sub> and water at 160 °C (the CO light off curve is in Fig. 3). The NO was released upon heating predominantly as NO in the low temperature regime with a NO desorption maximum spread between two release bands at ~200-300 °C. Thus, the 0.5 wt% Ru/ceria sample shows remarkable PNA properties even exceeding those of the best 1 wt% Pd/zeolite materials (direct comparison of their PNA performance shown in Fig. S1). Storage capacity of this sample is ~ 130 micromoles/g. NO<sub>x</sub>/Ru ratio is ~2.7. (see discussion *vide infra*). This could mean two potential things: either each ruthenium cation can adsorb 2 or more NO molecules or some of the NO stored on Ru in the presence of O<sub>2</sub> spills over onto ceria in the form of nitrites/nitrates. With the aid of FTIR (see discussion *vide infra*) we show that ruthenium mononitrosyl complex is formed under PNA conditions and that significant amounts of NO<sub>x</sub> spill over onto ceria in the form of nitrates under real conditions.

Since the hydrothermal stability of materials is of great importance, we hydrothermally aged Ru/Ceria at 750 °C in water/air steam for 10 hours, simulating the performance of catalysts used in diesel engines at the end of their useful life time. It is important to note that frequently in the literature Ru-containing materials (typically containing *not atomically dispersed* Ru but Ru/RuO<sub>x</sub> nanoparticles) are suggested to suffer from volatility issues [32,33] because of formation of extremely volatile and relatively toxic RuO<sub>4</sub> oxide. However, even after HTA at 750 °C the PNA performance of our Ru/ceria material remained essentially the same, thus surpassing even the hydrothermally stable and highly active Pd/SSZ-13 materials after hydrothermal aging (Fig. 3). [26]

This means that Ru/ceria does not volatilize and remains tightly attached to the surface. It is not surprising considering the fact the material was prepared via atom trapping approach in which ceria (with its strong trapping properties) traps Pt/Pd/Ru atoms on the surface that are stable at 800 °C. Despite the fact that NO<sub>x</sub> adsorption remains robust and essentially identical to the fresh sample, we observe changes to the CO oxidation performance of

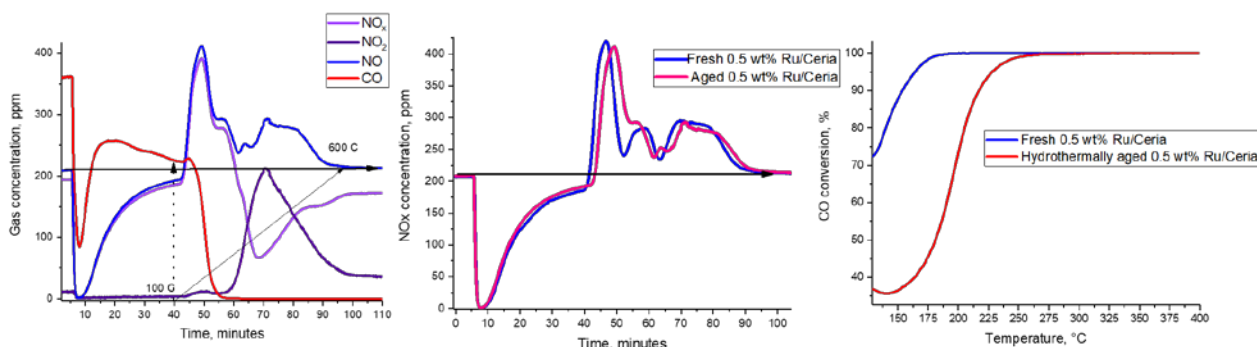


Figure 3. A. PNA performance of 0.5 wt% Ru/CeO<sub>2</sub> after aging at 750 °C/10hours/10% water vapor in air. B. Comparison of NO<sub>x</sub> profiles during PNA performance of fresh and aged 0.5 wt% Ru/CeO<sub>2</sub> (same PNA conditions as Fig. 2). Note that in the case of aged sample, temperature ramp was started ~2.2 minutes later and thus, the aged NO<sub>x</sub> release appears slightly shifted to the Right. C. Comparison of CO oxidation ability of the fresh and aged sample during PNA

Ru/ceria materials. More specifically, CO light off curve (Fig. 3) shows the shift of approximately  $\sim 75$  °C to higher temperatures. The fact that NO<sub>x</sub> adsorption performance remains the same while CO oxidation/adsorption performance changes suggests that NO<sub>x</sub> storage and CO oxidation are decoupled and occur independently (in other words, CO does not interfere with NO adsorption). The reasons behind CO oxidation activity deterioration are not fully understood at the moment and require

(performing so-called fast SCR, with an ideal 1:1 ratio between NO and NO<sub>2</sub> at temperatures  $\sim 270$  °C) and LNT (in this case, NO must first be oxidized to NO<sub>2</sub> in order to be stored on LNT materials). Best catalysts for NO oxidation typically contain expensive Pt and Pd [34-38]. Indeed, when we tested Pt and Pd atomically dispersed on ceria for NO oxidation (Figs. 4 and S5) these samples had pronounced activity. However, compared to state-of-the-art known materials they are much less active. We

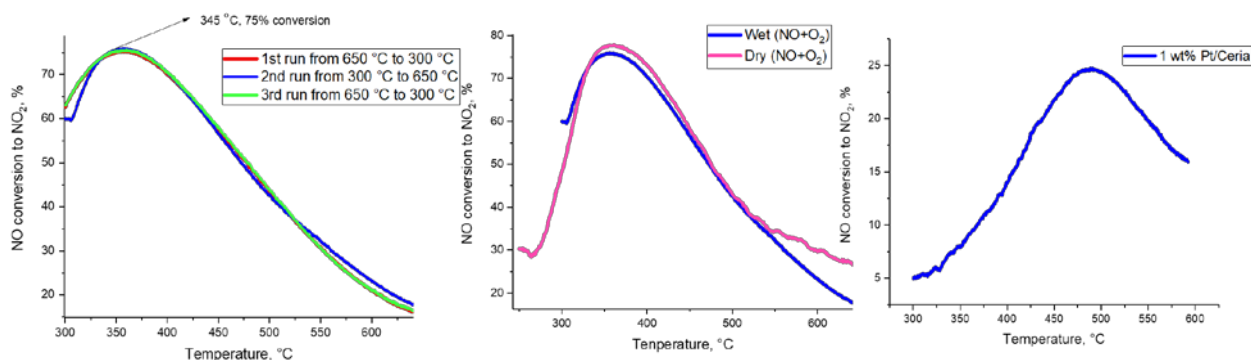


Figure 5. NO oxidation performance of A. 0.5 wt% HTA (hydrothermally aged) Ru/CeO<sub>2</sub> (3 continuous runs from 650 to 300, 300 to 650 and then 650 to 300 °C showing stable NO oxidation performance in the presence of  $\sim 3\%$  H<sub>2</sub>O, 120 mg catalyst, 470 ppm NO, 13% O<sub>2</sub>, total flow 300 sscm/min, GHSV  $\sim 150$  L/g\*hr. B. Comparison wet and dry NO oxidation going up in temperature to 650 °C. C. 1 wt% HTA Pt/CeO<sub>2</sub> sample NO oxidation performance under dry conditions with the same GHSV and NO/O<sub>2</sub> content as in A-B. NO oxidation for Pd/ceria sample is shown in Fig. S5.

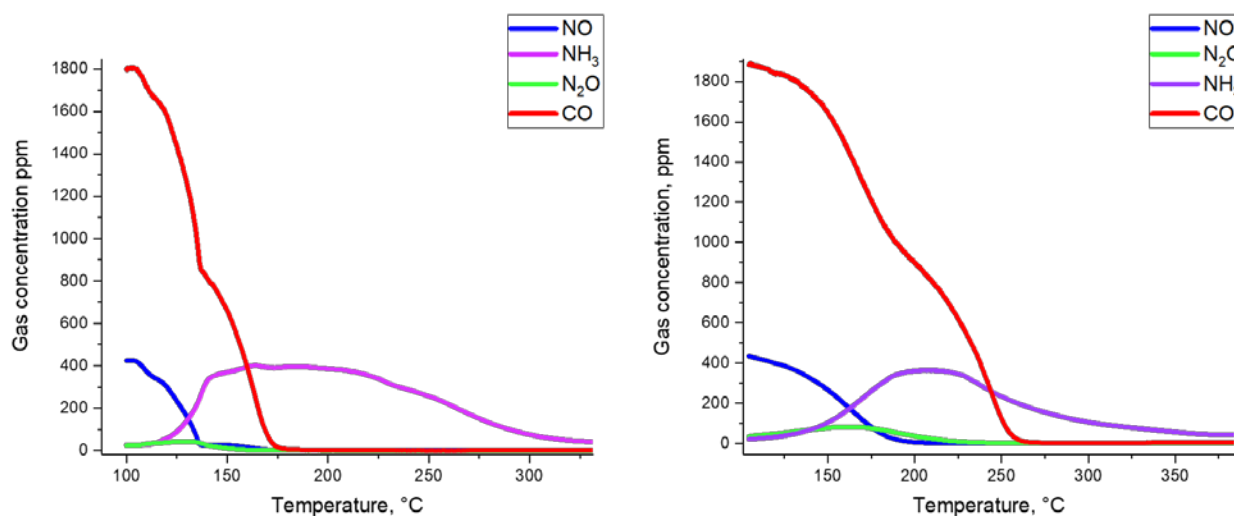


Figure 4. TWC performance of 0.5 wt% Ru/CeO<sub>2</sub> (left graph) and 0.1 wt% Ru/CeO<sub>2</sub> (Right graph). 120 mg catalyst, 300 sscm/min total flow, GHSV  $\sim 150$  L/G\*hr, 470 ppm NO, 1850 ppm CO,  $\sim 3\%$  H<sub>2</sub>O balanced in N<sub>2</sub>. Performance of 0.5 wt% Ru/CeO<sub>2</sub> sample under dry conditions is shown in Fig. S4.

further investigation: changes to the ceria surface (and its hydroxylation) and/or ceria facets in the presence of water vapor at such harsh temperature (750 °C) for extended time may be the reason behind this phenomenon.

Interestingly, at higher temperatures NO conversion to NO<sub>2</sub> even under typical vehicle exhaust conditions was observed. This prompted us to investigate atomically dispersed M/Ceria materials for NO oxidation (Fig. 4). We note that such studies have not been performed before on these materials. The reason why NO oxidation is of great importance for environmental catalysis is because NO<sub>2</sub> formation is important in lean NO<sub>x</sub> reduction [34-38] and because NO<sub>2</sub> facilitates ammonia SCR

then tested hydrothermally aged 0.5 wt% Ru/ceria sample in the wet NO/O<sub>2</sub>/N<sub>2</sub> stream (Fig. 4). The sample shows stable performance with little hysteresis going down, up and then back down in temperature (from 650 °C to 300 °C). Activity maximum is observed at  $\sim 350$  °C, with  $\sim 76\%$  conversion of NO, comparing very favourably with commercial DOC materials tested under similar conditions (they show maximum NO<sub>x</sub> conversion  $< 65\%$  under similar industrially relevant conditions in the dry feed) [38]. We also tested this sample in the dry NO oxidation (Fig. 4) and did not observe any prominent water influence on the NO oxidation activity.

All these results suggest that 0.5 wt% Ru/ceria sample is a notably robust PNA material with advantageous performance compared with state of the art 1 wt% Pd/zeolite sample. The price of ruthenium is 7-8 times cheaper than Pd, and the price of ceria is significantly lower than that of zeolite SSZ-13. Moreover, compared with Pd and Pt analogous materials, Ru/ceria offers

solid heterogeneous Ru supported catalysts and their NO ( $\text{NO}+\text{O}_2$ ) interactions as well as interactions with CO probe molecules [43-46]. We, therefore, studied CO and NO adsorption with FTIR on 0.5 wt% Ru/ceria sample. CO adsorption (Figs. S2,S3) on the sample produces lack of metallic CO bands for Ru and reveals the presence of  $\text{Ru}(\text{CO})_2$  and  $\text{Ru}(\text{CO})_3$  complexes on

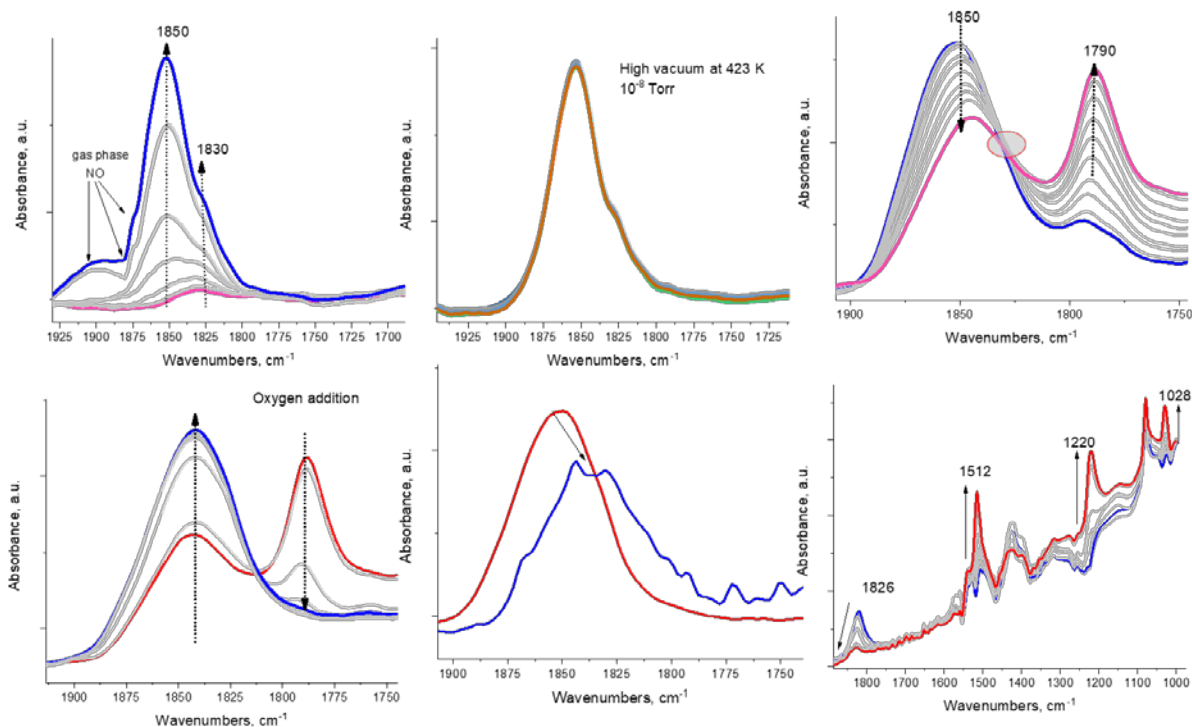


Figure 6. A. NO adsorption (0.5 Torr equilibrium pressure) at 298 K B. High vacuum after NO adsorption at 423 K C. Heating Ru-NO from 150 to 220 °C D. Introducing  $\text{O}_2$  at 220 °C after heating Ru-NO E. Water adsorption on Ru-NO complex at 120 °C F Ru-NO heated in the presence of  $\text{O}_2+\text{H}_2\text{O}$  from 120 to 350 °C: Ru-NO diminishes and chelating nitrates form (bands at 1512, 1220 and 1028  $\text{cm}^{-1}$ ).

higher NO oxidation activity than commercial Pd/Pt containing DOC formulations [38]. This provides an opportunity to utilize stable Ru/ceria materials for these applications. To confirm the versatility of Ru/ceria materials for NO<sub>x</sub> related environmental catalysis, we now turn our attention to another challenging reaction for gasoline engines called three-way-catalysis (TWC). TWC materials should perform catalytic removal of NO<sub>x</sub> in the presence of CO and water vapor under stoichiometric conditions [39-42]. We recently discovered that the true catalytically active species for low temperature TWC formulations [42] are isolated Rh(I) atoms (they cycle between I and III oxidation state during TWC) and we prepared very active and robust Rh/ceria materials for TWC applications with complete NO<sub>x</sub> conversion < 150 °C and Rh loadings 0.1 wt%. Since Ru(II) and Rh(I) are isostructural and isoelectronic d<sup>8</sup> metal species, yet Ru is ~ 27 times cheaper than Rh currently, we decided to explore the activity of 0.5 wt% Ru/ceria and 0.1 wt% Ru/Ceria samples for TWC in order to understand whether our synthesis route for Rh/Ceria TWC can be generalized and extended to other metals. Notably, these much cheaper Ru/ceria formulations show excellent performance in TWC under industrially relevant conditions (Fig. 5). Even the sample with only 0.1 wt% Ru shows >90% NO<sub>x</sub> conversion ~ 170 °C.

Despite the importance of Ru-containing materials for various NO-related catalytic processes, to our surprise we found only a handful characterization (more specifically FTIR) studies of any

the surface (Fig. 6). Adsorption of NO produces a sharp band due to NO interaction with cationic NO complex of Ru at ~1,850  $\text{cm}^{-1}$ , the minor 1830  $\text{cm}^{-1}$  band is due to presence of Ru cations on a different site on the ceria surface (Fig. 6). At higher temperatures in the absence of oxygen this band begins to decline with a new band growing at ~ 1790  $\text{cm}^{-1}$  and a clear isosbestic point indicating the simple stoichiometric transition of 1 Ru-NO complex into another. We suggest that this occurs due to vacancy formation in the vicinity of the Ru atom. However, as soon as we add oxygen to this system at this temperature, the vacancy is healed, and the initial NO band fully restores, fully confirming our suggestion. This NO band is incredibly robust under high vacuum at 150 °C and does not completely disappear even at 350 °C. In the presence of water, the NO band shifts to lower wavenumbers, the phenomenon that has been previously described for Pd/SSZ-13 and Pd/ZSM-5 and due to co-coordination of water and NO to the same Pd ion [47-49]. We note, for example, that coordination of water to isoelectronic Rh(I)(CO)<sub>2</sub> and Rh(I)(NO)<sub>2</sub> complexes shifts the CO and NO bands to the lower wavenumbers [50]. Simultaneously, in the presence of  $\text{O}_2/\text{NO}/\text{H}_2\text{O}$  in the IR cell, infrared spectra emerge after running this under PNA relevant temperatures (~from 120 to 350 °C), showing the decrease of ruthenium nitrosyl complex and chelating nitrate bands on the ceria surface. Thus, ruthenium helps store NO both as a nitrosyl complex and helps NO<sub>x</sub> be stored on the ceria surface due to

oxidation ability (as nitrites/nitrates) explaining high NO/Ru ratio which exceeds that of NO/Pd ratio of Pd in zeolites.

In summary, we disclose that among atomically dispersed M (Pt,Pd,Ru)/Ceria materials, inexpensive Ru/ceria catalysts show excellent performance for challenging pollutant abatement in both diesel and gasoline engines. The materials are stable and represent a new class of atomically dispersed materials based on Ru (~7 times cheaper than Pd and ~27 times cheaper than Rh) with immediate industrial applications. This opens up a possibility to introduce more sustainable ruthenium for catalytic and environmental applications instead of more expensive/environmentally less friendly Rh/Pt/Pd.

## Acknowledgements

The research at PNNL was supported by the U.S. Department of Energy, Energy Efficiency and Renewable Energy, Vehicle Technology Office. Experiments were conducted in the Environmental Molecular Sciences Laboratory (EMSL), a national scientific user facility sponsored by the Department of Energy's Office of Biological and Environmental Research at Pacific Northwest National Laboratory (PNNL). PNNL is a multi-program national laboratory operated for the DOE by Battelle Memorial Institute under Contract DE-AC06-76RL01830. We acknowledge the support of CLEERS (Crosscut Lean Exhaust Emissions Reduction Simulations). CLEERS is an initiative funded by the U.S. Department of Energy (DOE) Vehicle Technologies Office to support the development of accurate tools for use in the design, calibration, and control of next generation engine/emissions control systems that maximize efficiency while complying with emissions regulations.

\*Corresponding authors.

## Conflict of interest

The authors filed for a patent.

- Royal College of Paediatrics and Child Health. Every breath we take—the lifelong impact of air pollution. London: Royal College of Paediatrics and Child Health, 2016.
- N. R. Jaegers, J. K. Lai, Y. He, E. Walter, D. A. Dixon, M. Vasiliu, Y. Chen, C. M. Wang, M. Y. Hu, K. T. Mueller, I. E. Wachs, Y. Wang and J. Z. Hu, *Angew. Chem., Int. Ed.*, 2019, 131, 12739–12746.
- Ja-Hun Kwak, Russell G Tonkyn, Do Heui Kim, János Szanyi, Charles HF Peden, *J. Catal.*, 2010, 275, 187-190.
- I. Bull, A. Moini, G. Koermer, J. Patchett, W. Jaglowski, S. Roth, US Patent US20070134146A1, 2010.
- Zones, S.I. US Patent 4 544 538, 1985.
- T. Seiyama, T. Arakawa, T. Matsuda, N. Yamazoe, and Y. Takita, *Chem. Lett.*, 781 (1975)
- Chen, H.-Y.; Collier, J. E.; Liu, D.; Mantarosie, L.; Durán- Martín, D.; Novák, V.; Rajaram, R. R.; Thompsett, D. *Catal. Lett.* 2016, 146 (9), 1706–1711.
- Khivantsev, K.; Jaegers, N. R.; Kovarik, L.; Hanson, J. C.; Tao, F. (Feng); Tang, Y.; Zhang, X.; Koleva, I. Z.; Aleksandrov, H. A.; Vayssilov, G. N.; Wang, Y.; Gao, F.; Szanyi, J. *Angew. Chem.* 2018, 130 (51), 16914–16919.
- Khivantsev, K.; Jaegers, N. R.; Kovarik, L.; Prodinge, S.; Derewinski, M. A.; Wang, Y.; Gao, F.; Szanyi, J. *Appl. Catal. A. Gen.* 2019, 569, 141–148.
- Khivantsev, K.; Jaegers, N. R.; Koleva, I. Z.; Aleksandrov, H. A.; Kovarik, L.; Engelhard, M.; Gao, F.; Wang, Y.; Vayssilov, G. N.; Szanyi, J. *J. Phys. Chem. C* 2020, 124 (1), 309–321.
- Khivantsev, K.; Gao, F.; Kovarik, L.; Wang, Y.; Szanyi, J. *J. Phys. Chem. C* 2018, 122 (20), 10820–10827.
- Moliner, M.; Corma, A. *React. Chem. Eng.* 2019, 4 (2), 223–234.
- Khivantsev, K.; Jaegers, N. R.; Kovarik, L.; Hu, J. Z.; Gao, F.; Wang, Y.; Szanyi, J. *Emiss. Control Sci. Technol.* 2019. DOI: 10.1007/s40825-019-00139-w
- E. Bello, V. J. Margarit, E. M. Gallego, F. Schuetze, C. Hengst, A. Corma, M. Moliner, *Microporous and Mesoporous Materials* 302 (2020) 110222.
- K. Khivantsev, N. R. Jaegers, L. Kovarik, M. Wang, J. Z. Hu, Y. Wang, M. Derewinski, J. Szanyi, *Chemrxiv* 2020 DOI: 10.26434/chemrxiv.11821347
- Rajaram, R. R., Chen, H.-Y., Liu, D., US Patent US20150158019A1, 2015.
- Y. Ji, S. Bai and M. Crocker, *Appl. Catal., B*, 2015, 107–171, 283-292.
- Ji, Y.; Xu, D.; Bai, S.; Graham, U.; Crocker, M.; Chen, B.; Shi, C.; Harris, D.; Scapens, D.; Darab, J. *Ind. Eng. Chem. Res.* 2017, 56, 111–125.
- K Khivantsev, J Szanyi, NR Jaegers, L Kovarik, F Gao, Y Wang, US Patent App. 16/546,641
- L. Castoldi, R. Matarrese, S. Morandi, P. Ticali, Luca Lietti, *Catal. Today* 2020 doi.org/10.1016/j.cattod.2020.02.019
- A. Porta, T. Pellegrinelli, L. Castoldi, R. Matarrese, S. Morandi, S. Dzwigaj, L. Lietti, *Top. Catal.* 61 (2018) 2021–2034.
- Y. Ji, S. Bai, D. Xu, D. Qian, Z. Wu, Y. Song, R. Pace, M. Crocker, K. Wilson, A. Lee, D. Harris, D. Scapens, *Appl. Catal. B* 2019 doi: https://doi.org/10.1016/j.apcatb.2019.118499
- Ryou, Y. S.; Lee, J.; Cho, S. J.; Lee, H.; Kim, C. H.; Kim, D. *Appl. Catal. B Environ.* 2017, 212, 140–149.
- Ryou, Y. S.; Lee, J.; Lee, H.; Kim, C. H.; Kim, D. H., *Catal. Today* 2019, 320, 175–180.
- Lee, J.; Ryou, Y.; Hwang, S.; Kim, Y.; Cho, S. J.; Lee, H.; Kim, C. H.; Kim, D. H., *Catal. Sci. Technol.* 2019, 9 (1), 163–173.
- Kim, Y.; Hwang, S.; Lee, J.; Ryou, Y. S.; Lee, H.; Kim, C. H.; Kim, D. H. *Emiss. Control Sci. Technol.* 2019, 5 (2), 172–182.
- K. Khivantsev, X. Wei, L. Kovarik, N. R. Jaegers, E. D. Walter, P. Tran, Y. Wang, J. Szanyi, *Chemrxiv* 2020 DOI: 10.26434/chemrxiv.12385577
- Pereira-Hernandez, X. I.; DelaRiva, A.; Kunwar, D.; Xiong, H.; Sudduth, B.; Engelhard, M.; Kovarik, L.; Murayev, V.; Hensen, E.; Wang, Y.; Datye, A. K. *Nat. Commun.* 2019, DOI: 10.1038/s41467-019-09308-5
- Datye, A.; Wang, Y. *Natl. Sci. Rev.* 2018, 5, 630–632.
- Jones, J.; Xiong, H.; DeLaRiva, A. T.; Peterson, E. J.; Pham, H.; Challa, S. R.; Qi, G.; Oh, S.; Wiebenga, M. H.; Pereira Hernandez, X. I.; Wang, Y.; Datye, A. K. *Science* 2016, 353, 150–154.
- Nie, L.; Mei, D.; Xiong, H.; Peng, B.; Ren, Z.; Hernandez, X. I. P.; DeLaRiva, A.; Wang, M.; Engelhard, M. H.; Kovarik, L.; Datye, A. K.; Wang, Y., *Science* 2017, 358, 1419.
- Twigg, M.V., Haren Gandhi 1941-2010: Contributions to the Development and Implementation of Catalytic Emissions Control Systems. *Platinum Metals Review*, 2011. 55(1): p. 43-53.
- Warlimont, H.; W.E. Martienssen, eds. *Springer Handbook of Condensed Matter and Materials Data*. 2006.
- M. Koebel, M. Elsener, M. Kleemann, *Catal. Today* 59,335 (2000).
- N. Takahashi et al., *Catal. Today* 27, 63 (1996).
- M. Koebel, G. Madia, M. Elsener, *Catal. Today* 73, 239 (2002).
- P. Bourges, S. Lunati, G. Mabilon, *Catalysis And Automotive Pollution Control IV* 116, 213 (1998)
- C. H. Kim, G. Qi, K. Dahlberg, W. Li, *Science*, 327, pp. 1624-1627.
- Harrison, B, Diwell, AF, Hallett, C. Promoting platinum metals by ceria. *Platinum Metals Rev*1988; 32: 73–83.

- (40) Taylor, K. *Catal. Rev.: Sci. Eng.* 1993, 35 (4), 457–481.
- (41) Granger, P.; Parvulescu, V. I. *Chem. Rev.* 2011, 111.
- (42) K. Khivantsev, C. Vargas, J. Tian, L. Kovarik, N. R. Jaegers, J. Szanyi, Y. Wang, Chemrxiv 2020 DOI: 10.26434/chemrxiv.12086004
- (43) H. Landmesser, H. Miessner *J. Phys. Chem.* 1991, 95, 26, 10544–10546
- (44) Hadjiivanov, K.; Lavalley, J.-C.; Lamotte, J.; Mauge, F.; SaintJust, J.; Che, M. *J. Catal.* 1998, 176, 415.
- (45) H. Miessner, *J. Am. Chem. Soc.* 1994, 116, 11522–11530.
- (46) Miessner, H.; Richter, K. *J. Mol. Catal. A-Chem.* 1999, 146, 107–115.
- (47) Chen, H.-Y.; Collier, J. E.; Liu, D.; Mantarosie, L.; Durán- Martín, D.; Novák, V.; Rajaram, R. R.; Thompsett, D. *Catal. Lett.* 2016, 146 (9), 1706–1711.
- (48) Chakarova K, Ivanova E, Hadjiivanov K, Klissurski D, Knozinger H (2004) *Phys Chem Chem Phys* 6:3702.
- (49) J.Lee, J. Kim, Y. Kim, S. Hwang, H. Lee, C. H. Kim, D. H. Kim, *Appl. Catal. B*, 2020, 277, 119190
- (50) K. Khivantsev, PhD Thesis, University of South Carolina, 2015.

# Identification of Ru/Ceria among single atom doped ceria materials as a stable and superior catalyst for abatement of diesel and gasoline engine pollutants

Konstantin Khivantsev,<sup>a\*</sup> Nicholas R. Jaegers,<sup>a</sup> Libor Kovarik,<sup>a</sup> Jinshu Tian<sup>a</sup>, Xavier Isidro Pereira Hernandez,<sup>a</sup> Yong Wang<sup>a,b\*</sup> and János Szanyi<sup>a\*</sup>

## Supplementary Information

### Materials and Methods

Cerium nitrate hexahydrate was purchased from Sigma with purity of 99.999%. Ceria nanoparticles were prepared from it by heating in a regular muffle furnace under static conditions at 550 °C for 5 hours in accordance with the previous studies [29-31]. Ruthenium nitrosyl nitrate solution was purchased from Sigma and used as is. To prepare the loadings of Ru on ceria of 0.1 and 0.5 wt%, the desired amount of Ru precursor solution was dissolved in the minimum amount of water (total volume approximately equivalent to the pore volume of ceria) and added with a micropipette to the desired amount of ceria while continuously stirring with the spatula to ensure uniformity. The obtained wetted powder was dried under N<sub>2</sub> flow at 80 °C, and then calcined at 800 °C for 1 hour in a regular muffle furnace with a ramp rate of 5 °C/min. The as-prepared 0.1 and 0.5 wt% Ru/Ceria powders were pressed, crushed and sieved to 60-80 mesh, and subsequently used as catalysts. Samples with 0.5 and 1 wt% loading of Pd and Pt, respectively, were prepared in a way identical to the Ru/ceria sample. Pd and Pt terramine nitrate salts (Sigma) were used as Pd and Pt precursors.

Na/SSZ-13 zeolite with Si/Al ~ 6 was hydrothermally synthesized using the following recipe: 0.8 g of NaOH (Sigma Aldrich, ≥ 99%) was dissolved in 50 ml of deionized water. Then, 17 g of TMAOH (Sachem Inc., 25% N,N,N-trimethyl-1-adamantyl ammonium hydroxide) was added as structure directing agent. Consequently, 1.5 g of Al(OH)<sub>3</sub> (Sigma Aldrich, ~54% Al<sub>2</sub>O<sub>3</sub>) was slowly added to the solution and stirred at 400 rpm until it was completely dissolved. Afterwards, 20.0 g of LUDOX HS-30 colloidal silica (Sigma Aldrich, 30 wt% suspension in H<sub>2</sub>O) was added slowly to the solution until a uniform white gel was formed. The obtained gel was sealed in a 125 mL Teflon-lined stainless steel autoclave containing a magnetic stir bar. Hydrothermal synthesis was carried out at 160°C under continuous gel stirring at 400 rpm for 4 days. After synthesis, the zeolite cake was separated from the suspension by centrifugation and washed thoroughly with deionized water. It was then dried at 80°C under N<sub>2</sub> flow overnight and calcined in air at 550°C for 5 h in order to remove the SDA. NH<sub>4</sub>/SSZ-13 was obtained by ion exchange

of the as-prepared Na/SSZ-13 zeolite with 0.5 M  $\text{NH}_4\text{NO}_3$  solution at 80°C for 5 h. The process was repeated three times.

Pd/Zeolite powders with desired loading of Pd (1 wt%) was obtained via modified incipient wetness impregnation method, described by us earlier, with Pd(II) tetramine nitrate solution (10 wt %, Sigma) and  $\text{NH}_4$ -forms of zeolites. Benefits of using palladium (II) tetra-amine nitrate precursor versus palladium nitrate as well as  $\text{NH}_4$ -forms of zeolite were previously described in detail [8,11]. They were subsequently dried at 80°C and subsequently calcined at 650°C in static air. More specifically a minimum amount of the Pd(II) precursor solution was added to zeolite in the amount approximately equivalent to the total pore volume of the zeolite. The thick paste was mixed for 30 minutes, followed by calcination in air at 650°C for 5 h (ramping rate 2°C/min).

Hydrothermal aging (HTA) was performed at 750 °C for 10 hours in a flow reactor with GHSV ~ 150 L/g\*hr. The gas mix, used for HTA, containing air and 10%  $\text{H}_2\text{O}$  in air.

(NO+CO) catalytic experiments were conducted in a plug-flow reactor system with powder samples (120 mg, 60–80 mesh) loaded in a quartz tube, using a synthetic gas mixture containing 460 ppm of NO and 1,750 ppm CO balanced with  $\text{N}_2$  at a flow rate of 310 sccm (corresponding to GHSV 150 L/g\*hr). Wet experiments were performed in the presence of 2.6 % water vapor. All the gas lines were heated to over 100 °C. Concentrations of reactants and products were measured by an online MKS MultiGas 2030 FTIR gas analyzer with a gas cell maintained at 191 °C. Two four-way valves were used for gas switching between the reactor and the bypass. Heating and cooling rates were 2 K/min.

Standard  $\text{NO}_x$  adsorption tests were conducted in a plug-flow reactor system with powder samples (120 mg, 60–80 mesh) loaded in a quartz tube, using a synthetic gas mixture that contained ~200 ppm of  $\text{NO}_x$ , CO (360 ppm), 14%  $\text{O}_2$ , 3%  $\text{H}_2\text{O}$  balanced with  $\text{N}_2$  at a flow rate of 300 sccm at 100 °C. All the gas lines were heated to over 100 °C. Concentrations of reactants and products were measured by an online MKS MultiGas 2030 FTIR gas analyzer with a gas cell maintained at 191°C. GHSV for all the adsorption/desorption experiments was 150 L/g\*hr. Heating rate was 10 K/min.

NO oxidation experiments were conducted in the same plug-flow reactor system in the presence and absence of water. 120 mg of desired catalyst were loaded, and the experiments were performed in the presence of 460 ppm NO, ~3% water, 13%  $\text{O}_2$  balanced with nitrogen. Heating and cooling rates were 2 K/min.

BET surface areas were conducted on a Micromeritics ASAP-2000 instrument with Ar as the adsorbate. Prior to analysis, the samples were dehydrated under vacuum for 3 hours at 250 °C.

HAADF-STEM analysis was performed with an FEI Titan 80-300 microscope operated at 300 kV. The instrument is equipped with a CEOS GmbH double-hexapole aberration corrector

for the probe-forming lens which allows for imaging with 0.1 nm resolution in scanning transmission electron microscopy mode (STEM). The images were acquired with a high angle annular dark field (HAADF) detector with inner collection angle set to 52 mrad. The powder samples were loaded into the sample holder. The images were collected in various projections and imaged immediately to minimize beam damage during the experiment.

The *in situ* transmission IR experiments were conducted in a home-built cell housed in the sample compartment of a Bruker Vertex 80 spectrometer, equipped with an MCT detector and operated at 4 cm<sup>-1</sup> resolution. The powder sample was pressed onto a tungsten mesh which, in turn, was mounted onto a copper heating assembly attached to a ceramic feedthrough. The sample could be resistively heated, and the sample temperature was monitored by a thermocouple spot welded onto the top center of the W grid. The cold finger on the glass bulb containing CO was cooled with liquid nitrogen to eliminate any contamination originating from metal carbonyls, while NO was cleaned with multiple freeze–pump–thaw cycles. Prior to spectrum collection, a background with the sample in the IR beam was collected. Each spectrum reported is obtained by averaging 64 scans.

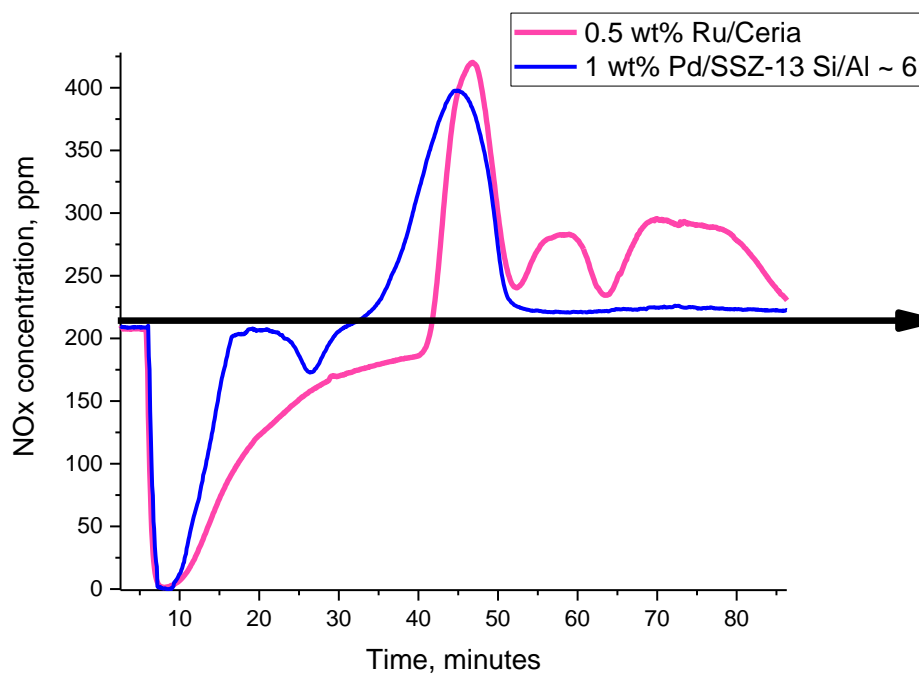


Figure S1. Comparison of PNA performance of 0.5 wt% Ru/Ceria and 1 wt% Pd/SSZ13 with Si/Al ~ 6. PNA was performed at 100 °C at GHSV ~ 150 L/g\*h and conditions identical to Figs. 1 and 2. Note in the case of Pd/SSZ-13, ramp rate of 10 K/min was started at the 15 min mark, while for 0.5 wt% Ru/Ceria sample it was started at the 36 min mark.

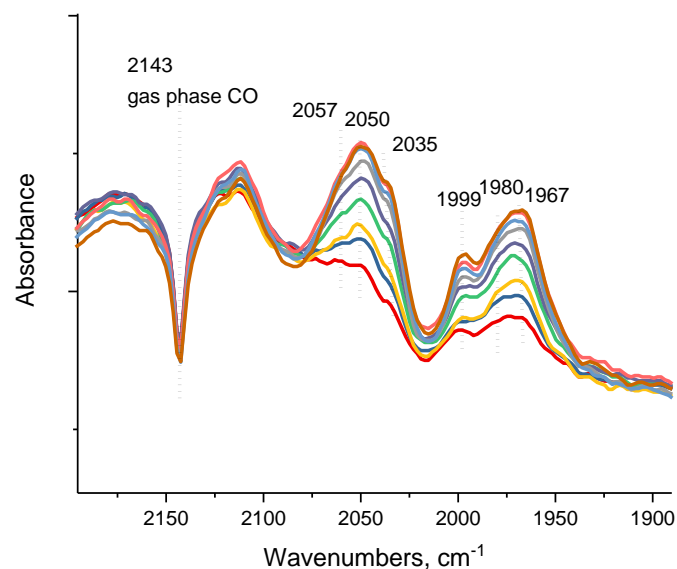


Figure S2. FTIR during CO adsorption (0.7 Torr equilibrium pressure) on 0.5 wt% Ru/ceria.

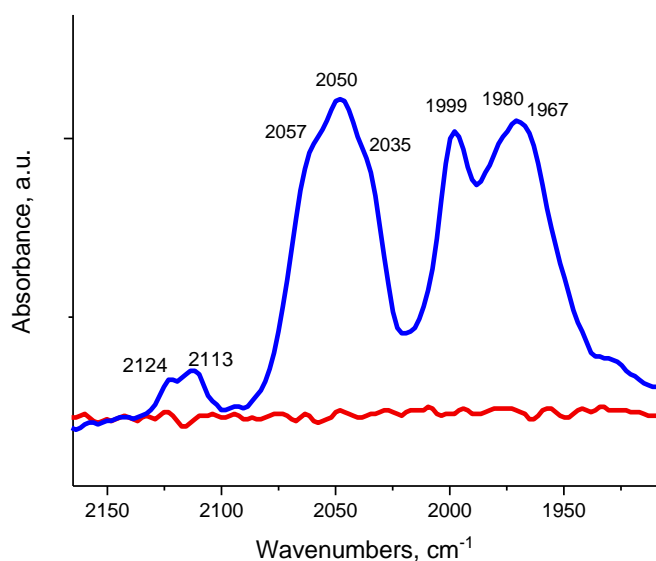


Figure S3. FTIR showing the CO region after applying high vacuum on the sample in Fig. S2. The bands at 2124 and 2113  $\text{cm}^{-1}$ , obscured by the gas-phase CO bands in Fig. S2, are visible in this spectrum. The observed band-structure is very similar to Ru(II)/Zeolite system after CO adsorption, in which a mixture of di- and tri-carbonyls of Ru forms.

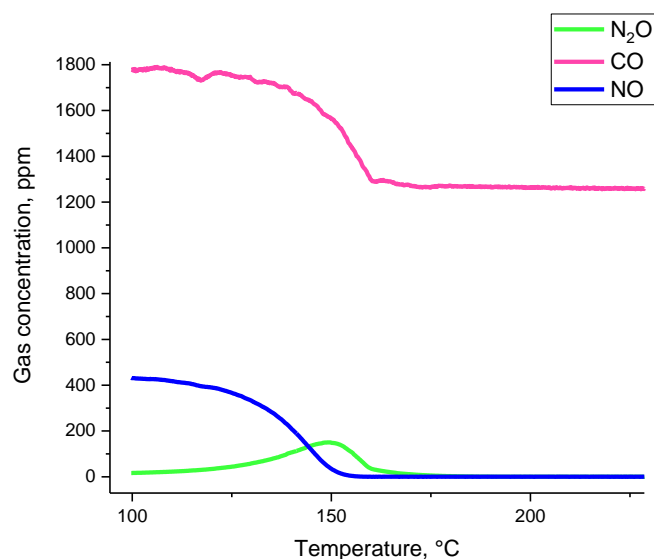


Figure S4. TWC performance of 0.5 wt% Ru/CeO<sub>2</sub> for dry CO+NO reaction. 120 mg catalyst, 300 sscm/min total flow, GHSV ~ 150 L/g\*hr, 470 ppm NO, 1800 ppm CO, balanced in N<sub>2</sub>.

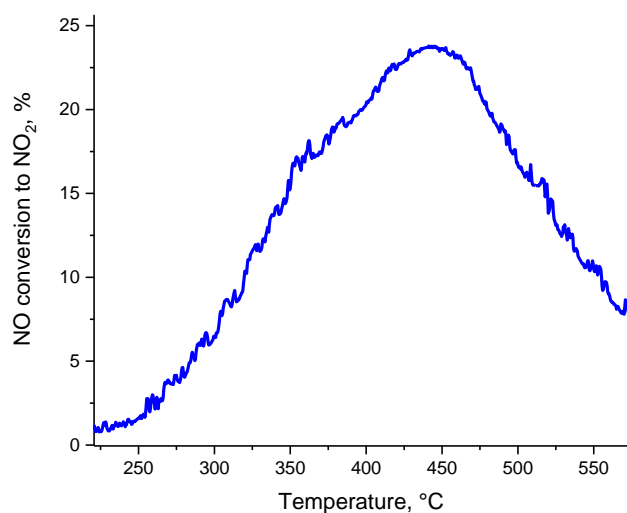


Figure S5. NO oxidation performance of 0.5 wt% Pd/CeO<sub>2</sub>. 120 mg catalyst, 300 sscm/min total flow, GHSV ~ 150 L/g\*hr, 470 ppm NO, 13% O<sub>2</sub>, balanced in N<sub>2</sub>.

Table S1. BET Surface areas of various synthesized samples.

Sample	BET area, m <sup>2</sup> /g
Ceria	98
Ceria calcined 800 °C	11
0.5 Ru/Ceria calcined 800 °C	44
1 Pt/Ceria calcined 800 °C	38
0.5 Pd/Ceria calcined 800 °C	36
0.1 Ru/Ceria calcined 800 °C	40